SMU
SINGAPORE MANAGEMENT UNIVERSITY

Lee Kong Chian School of Business

QF620 Stochastic Modelling in Finance

Project Report by Section G1 Team 1

Authors

Chan Ric
Kevin Montana Wongso
Nguyen Thanh Binh
Wong Jia Shing
Yash Ashish Kumar Joshi
Zhang Yinliang

Part I (Analytical Option Formulae)

A vanilla option is a financial instrument that gives the holder the right, but not the obligation, to buy or sell an underlying asset at a predetermined price within a given timeframe. This option is a call/put option that has no special nor unusual features, meaning it is standardised if traded on an exchange, e.g., SGX. On the other hand, a digital cash/asset-or-nothing call (resp. put) is an option that has a binary outcome: it pays out either a fixed amount of one unit of cash/asset, if the underlying stock becomes above (resp. below) a predetermined threshold or strike price, or pays out nothing.

Let $Z \sim N(0,1)$ be the standard normal random variable, whose probability density function (PDF) is given by $\phi(z) = \frac{1}{\sqrt{2\pi}} e^{-\frac{z^2}{2}}$. Define its cumulative distribution function (CDF) by $\Phi(z) = \int_{-\infty}^{z} \phi(z')\, dz'$.

In the displaced-diffusion model, the factor $\beta \in [0,1]$ plays a significant role in modifying the underlying asset's price S_0's dynamics, meaning β controls the degree to which S_0 influences the asset's volatility:

- $\beta = 1$: The model reduces to the standard Black-Scholes model, where the volatility term is simply σS_0, meaning the volatility is proportional to the asset's/stock's price.
- $\beta = 0$: The model's dynamics are dominated by the constant F_0, making the volatility independent of the asset's/stock's price. This implies the volatility term becomes σF_0.
- $0 < \beta < 1$: The model incorporates a blend of both the asset's/stock's price S_0 and the constant F_0. This allows the model to capture scenarios where the volatility is not entirely proportional to the asset's/stock's price but is also influenced by some baseline, represented by F_0.

In general, a higher β implies the volatility is more strongly tied to the asset's/stock's price, while a lower β suggests the volatility is more dependent on the constant F_0. This flexibility makes the displaced-diffusion model useful in modelling situations where the asset's/stock's price volatility does not behave purely as a linear function of its current price.

We first define the following variables:

t: the time in years, where $t \geq 0$; assuming WLOG that $t = 0$ represents the current year,

r: the annual continuously compounded risk-free interest rate,

S_0: the initial asset/stock price,

μ: the annual drift rate of S_0,

σ: the standard deviation of the stock's returns, i.e., the square root of the quadratic variation of the stock's log price process (measure of stock's volatility),

T: the expiry date of the option, i.e., $0 \leq t \leq T$.

K: the at-the-money (ATM) strike price of the option,

F_0: the initial discounted futures price ($F_0 = S_0 e^{rT}$).

Using these definitions, we derive (see `part1.ipynb`) and define the following equations for the prices of the European options at expiry date T under the respective option pricing models:

Model	Option type		
	Vanilla call/put	Digital cash-or-nothing call/put	Digital asset-or-nothing call/put
Black-Scholes $d_1 = \frac{\log\frac{S_0}{K} + \left(r + \frac{\sigma^2}{2}\right)T}{\sigma\sqrt{T}}$ $d_2 = d_1 - \sigma\sqrt{T}$	Call: $C_{BS,v} = S_0\Phi(d_1) - Ke^{-rT}\Phi(d_2)$ Put: $P_{BS,v} = Ke^{-rT}\Phi(-d_2) - S_0\Phi(-d_1)$	Call: $C_{BS,c} = e^{-rT}\Phi(d_2)$ Put: $P_{BS,c} = e^{-rT}\Phi(-d_2)$	Call: $C_{BS,a} = S_0\Phi(d_1)$ Put: $P_{BS,a} = S_0\Phi(-d_1)$
Bachelier $d = \frac{S_0 - K}{\sigma\sqrt{T}}$	$C_{Ba,v} = e^{-rT}\left[(S_0 - K)\Phi(d) + \sigma\sqrt{T}\phi(d)\right]$ $P_{Ba,v} = e^{-rT}\left[(K - S_0)\Phi(-d) + \sigma\sqrt{T}\phi(-d)\right]$	$C_{Ba,c} = e^{-rT}\Phi(d)$ $P_{Ba,c} = e^{-rT}\Phi(-d)$	$C_{Ba,a} = S_0\Phi(d) + \sigma\sqrt{T}\phi(d)$ $P_{Ba,a} = S_0\Phi(-d) + \sigma\sqrt{T}\phi(-d)$
Black $d_1 = \frac{\log\frac{F_0}{K} + \frac{\sigma^2}{2}T}{\sigma\sqrt{T}}$ $d_2 = d_1 - \sigma\sqrt{T}$	$C_{B,v} = e^{-rT}\left[F_0\Phi(d_1) - K\Phi(d_2)\right]$ $P_{B,v} = e^{-rT}\left[K\Phi(-d_2) - F_0\Phi(-d_1)\right]$	$C_{B,c} = e^{-rT}\Phi(d_2)$ $P_{B,c} = e^{-rT}\Phi(-d_2)$	$C_{B,a} = F_0e^{-rT}\Phi(d_1)$ $P_{B,a} = F_0e^{-rT}\Phi(-d_1)$
Displaced-diffusion $d_1 = \frac{\log\left(\frac{F_0}{F_0 + \beta(K - F_0)}\right) + \frac{(\sigma\beta)^2}{2}T}{\sigma\beta\sqrt{T}}$ $d_2 = d_1 - \sigma\beta\sqrt{T}$	$C_{D,v} = C_{B,v}\left(\frac{F_0}{\beta}, K + \frac{1-\beta}{\beta}F_0, r, \beta\sigma, T\right)$ $= e^{-rT}\left[\frac{F_0}{\beta}\Phi(d_1) - \left(K + \frac{1-\beta}{\beta}F_0\right)\Phi(d_2)\right]$ $P_{D,v} = P_{B,v}\left(\frac{F_0}{\beta}, K + \frac{1-\beta}{\beta}F_0, r, \beta\sigma, T\right)$ $= e^{-rT}\left[\left(K + \frac{1-\beta}{\beta}F_0\right)\Phi(-d_2) - \frac{F_0}{\beta}\Phi(-d_1))\right]$	$C_{D,c} = e^{-rT}\Phi(d_2)$ $P_{D,c} = e^{-rT}\Phi(-d_2)$	$C_{D,a} = \frac{F_0}{\beta}\Phi(d_1)$ $P_{D,a} = \frac{F_0}{\beta}\Phi(-d_1)$

These models are used to evaluate different types of options under varying assumptions about the underlying asset's volatility, time to maturity, and the relationship between volatility and the asset price. Our key focus here is on how the underlying assumptions affect the option prices.

Substituting $K = 85$, $r = 5\% = 0.05$, $\sigma = 0.40$, $T = 0.2$ and $\beta = 0.3$ into the equations defined above, we compute each of the option prices using Python and obtain the following results:

S_0	$C_{BS,v}$	$P_{BS,v}$	$C_{BS,c}$	$P_{BS,c}$	$C_{BS,a}$	$P_{BS,a}$	$C_{Ba,v}$	$P_{Ba,v}$	$C_{Ba,c}$	$P_{Ba,c}$	$C_{Ba,a}$	$P_{Ba,a}$
80	4.005	8.159	0.351	0.639	33.861	46.139	0	4.950	0	0.990	0	80
90	9.560	3.714	0.606	0.384	61.109	28.891	4.950	0	0.990	0	90	0

S_0	$C_{B,v}$	$P_{B,v}$	$C_{B,c}$	$P_{B,c}$	$C_{B,a}$	$P_{B,a}$	$C_{D,v}$	$P_{D,v}$	$C_{D,c}$	$P_{D,c}$	$C_{D,a}$	$P_{D,a}$
80	4.005	8.159	0.351	0.639	33.861	46.139	3.913	8.067	0.373	0.617	105.857	160.81
90	9.560	3.714	0.606	0.384	61.109	28.891	9.705	3.859	0.627	0.363	195.909	104.091

The table demonstrates how different models handle the pricing of both vanilla and digital options, illustrating how volatility and the relationship between the asset price and volatility can affect option values. Under the Black-Scholes model applied to the vanilla options, we see that for a lower initial stock price ($S_0 = 80$), the call option is cheaper, while the put option is more expensive. This is expected as the stock price is below the strike price ($K = 85$). Conversely, when the stock price rises above the strike price ($S_0 = 90$), the call option becomes more valuable while the put option becomes cheaper. On the other hand, digital options offer binary outcomes − either a fixed cash or asset payout if the option is in the money (the asset price crosses the strike price), or nothing otherwise. Specifically, the prices for cash-or-nothing options and asset-or-nothing options reflect the probabilities of these binary outcomes. These prices under different models vary depending on how each model captures volatility and the underlying asset's price dynamics. For example, under the Bachelier model, the prices for asset-or-nothing options are significant due to the model's assumption of a linear Brownian motion for asset prices. Finally, the prices calculated under the displaced-diffusion model show how introducing displacement affects the valuation of options. For instance, the prices for digital options under this model are different from those in the Black-Scholes model, highlighting the impact of β on option pricing. This property allows the displaced-diffusion model to capture situations where volatility does not strictly follow the asset price, offering a more flexible framework for option pricing. Overall, these insights help traders and risk managers choose the most appropriate model for their needs, depending on the asset's characteristics and the type of options being priced.

Part II (Model Calibration)

On `1-Dec-2020`, the S&P 500 (SPX) index value was 3662.45, while the SPDR S&P 500 Exchange Traded Fund (SPY) stock price was 366.02. The call and put option prices (bid & offer) over 3 maturities are provided in the spreadsheets `SPX_options.csv` and `SPY_options.csv`. The discount rate on this day is in the file `zero_rates_20201201.csv`. To obtain the market-implied volatility smile, we first compute it under the Black-Scholes model by extracting the implied volatilities from the option prices observed in the market. This process involves finding the volatility parameter σ in the Black-Scholes formulae that equate the theoretical option price to the market price for each strike price and maturity. The Black-Scholes formulae themselves assume constant volatility, but the variation in implied volatility across different strike prices, known as the volatility smile, reflects deviations from this assumption in real markets.

We start by gathering the relevant data for the S&P 500 index and its associated SPDR ETF options. This includes the option prices (both bid and offer) for several strike prices and maturities, as well as the risk-free discount rates for the respective maturities, provided in the `zero_rates_20201201.csv` file. Using the given SPX and SPY option price data from the provided spreadsheets (`SPX_options.csv`, `SPY_options.csv`), we proceed with the calculation of implied volatility. To do this, we reverse-engineer the Black-Scholes formulae. By solving numerically for σ using Brent's method (coded as `brentq`) as computed in our Jupyter Notebook, we obtain the implied volatility for each option. Once this is done across all available options, we plot these against the strike prices for each maturity as shown below.

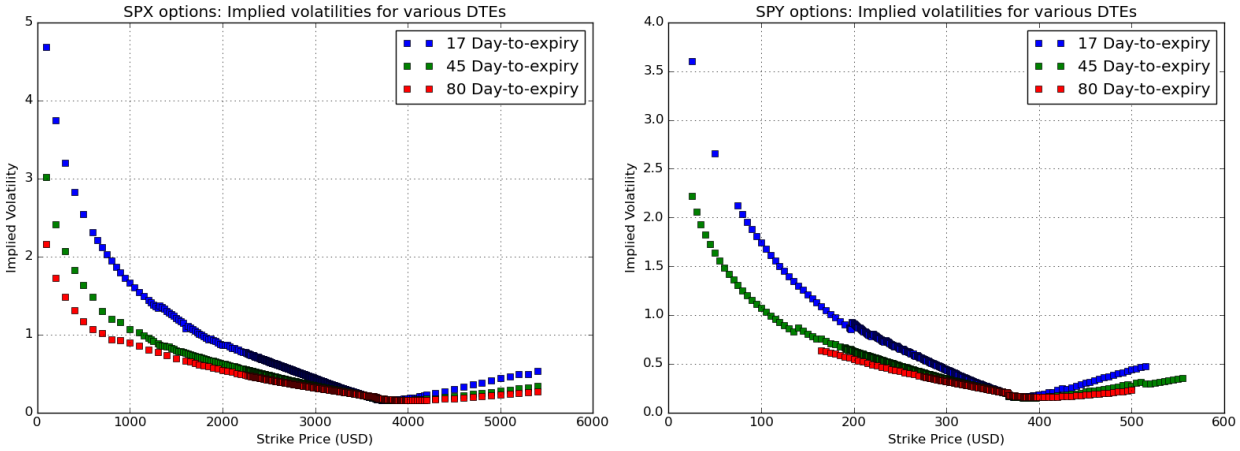

Here, we observe distinct market-implied volatility smiles for different maturities. In the Black-Scholes (log-normal) framework, implied volatility should theoretically remain constant across strike prices for a given maturity, assuming that the model's assumption of constant volatility holds. However, the graphs reveal a clear deviation from this assumption, as we see a pronounced smile or skew, indicating that implied volatility varies significantly with strike prices. From the SPX chart, we observe that for all maturities (17, 45 and 80 days), the implied volatility is significantly higher for lower strike prices and gradually decreases as the strike price increases, reaching a minimum around the at-the-money ATM strikes. Beyond the ATM region, the volatility starts increasing again slightly for higher strike prices, forming a typical volatility smile pattern. This pattern is most pronounced for shorter maturities (e.g., 17 days) and becomes flatter as the maturity increases. The SPY chart shows a similar pattern, though the scale of implied volatilities is lower compared to SPX. The implied volatility remains high for out-of-the-money (OTM) put options, reflecting a similar smile shape. Additionally, the skew is steeper for shorter maturities, especially at lower strike prices. This

suggests that the market is pricing in more risk or uncertainty for SPY options with shorter maturities and for strikes that are further from the current spot price.

The shape of the volatility smile in both cases allows us to infer important market expectations. Higher implied volatility for OTM options, particularly for puts, indicates that the market anticipates significant price movements or possible downside risk in the underlying asset. In contrast, the flatter slopes near ATM strikes suggests the market expects relatively stable volatility near current levels. The skewed nature of the volatility smile suggests an asymmetric view of risk, where the market might be hedging against large downward movements in price, especially for shorter-dated options. These observations reflect the market's expectations of future volatility and risk. The pronounced skew in shorter maturities points to heightened uncertainty or anticipated market movements in the near term, particularly at lower strike prices. These observations provide critical insights that inform more sophisticated option pricing models, such as the displaced-diffusion and SABR models, which address the limitations of the lognormal assumption of constant volatility.

Next, to match the option prices, we calibrate both models: displaced-diffusion and SABR ($\beta = 0.7$). The SABR volatility and two error equations are defined in `part2.ipynb`. To optimize the calibration accuracy, we use the `least_squares` algorithm in the `scipy` module to calibrate the displaced-diffusion and SABR model parameters by minimising the sum of squared error terms, i.e., via $\min_{\sigma,\,\beta} \sum_{i=1}^{n}(\epsilon_i^D)^2$ and $\min_{\alpha,\,\rho,\,\nu} \sum_{i=1}^{n}(\epsilon_i^{\text{SABR}})^2$ respectively. The model parameters reported and implied volatility smile plots obtained are shown below:

	SPX, 17 days	SPX, 45 days	SPX, 80 days	SPY, 17 days	SPY, 45 days	SPY, 80 days
σ	0.174	0.185	0.194	0.201	0.197	0.200
β	1.498×10^{-7}	1.022×10^{-6}	2.66×10^{-13}	7.610×10^{-7}	6.560×10^{-9}	3.755×10^{-8}

Table 1: Calibrated values under the displaced-diffusion model

	SPX, 17 days	SPX, 45 days	SPX, 80 days	SPY, 17 days	SPY, 45 days	SPY, 80 days
α	1.212	1.817	2.140	0.665	0.908	1.121
ρ	-0.301	-0.404	-0.575	-0.412	-0.489	-0.633
ν	5.460	2.790	1.842	5.250	2.729	1.742

Table 2: Calibrated values under the SABR model

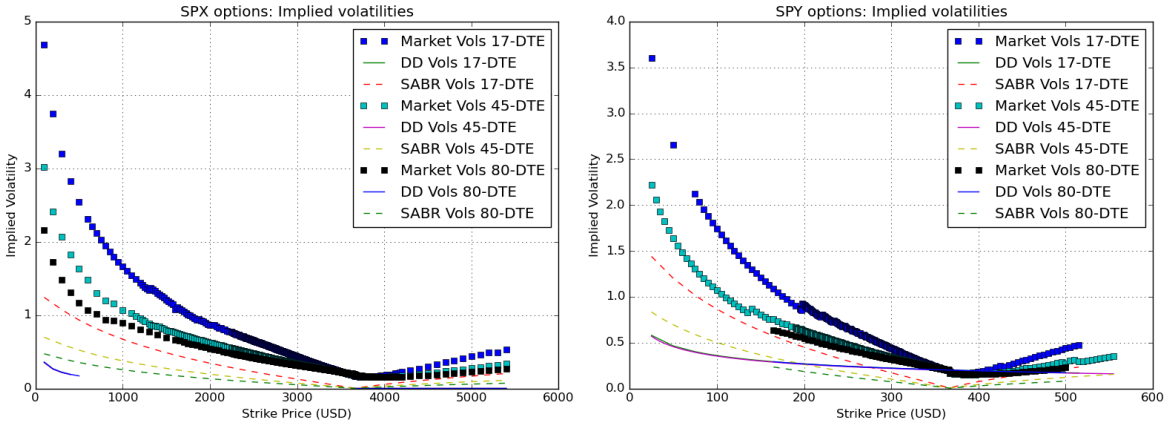

The shape of the implied volatility smile is significantly influenced by key parameters in the displaced-diffusion (DD) and SABR models, which address the limitations of the Black-Scholes framework. In the DD model, the parameter β controls the weighting between the underlying asset's price and its displacement. When $\beta = 1$, the model reduces to the Black-Scholes framework, assuming constant volatility. However, as β decreases, the smile becomes steeper, particularly for OTM and in-the-money (ITM) options, allowing the model to better capture deviations from the Black-Scholes assumptions. Conversely, higher β values result in a flatter smile, limiting the model's ability to capture the pronounced skew and curvature observed in real markets, especially for shorter-dated options. In the SABR model, the parameters ρ and ν provide additional flexibility to model implied volatility. The correlation parameter ρ affects the skewness of the smile, with negative ρ values producing a left-skewed smile, aligning with market phenomena such as the leverage effect. Positive ρ values, on the other hand, lead to more symmetric smiles. The volatility-of-volatility parameter ν introduces stochasticity, allowing the SABR model to replicate steep curvatures at OTM and ITM strikes for shorter maturities while adapting to flatter smiles for longer maturities. Together, ρ and ν enable the SABR model to capture the asymmetric risk perceptions and dynamic volatility clustering observed in market data.

A comparison of the implied volatility plots highlights the SABR model's superior ability to fit market data compared to the DD model. While the DD model introduces curvature to the smile, it struggles to replicate the pronounced skew and steepness at OTM strikes, particularly for short-dated options. The DD model's reliance on β limits its flexibility, as it cannot account for stochastic volatility or asymmetric clustering. This results in systematic underestimation of implied volatility at OTM puts and less accurate fits near at-the-money (ATM) strikes. Additionally, as option maturities increase, the DD model fails to adapt to the flattening of the smile, further highlighting its limitations. In contrast, the SABR model demonstrates greater adaptability and accuracy. By incorporating ρ and ν, the SABR model replicates the left skew seen in equity options, fitting both the extremes and the ATM region of the smile more effectively. The model captures the pronounced curvature of short-term options while maintaining consistency across longer maturities. For example, the SABR model closely matches market-implied volatilities for OTM puts and calls, even in environments of heightened demand for downside protection or significant market uncertainty.

In conclusion, while the DD model provides a practical improvement over the Black-Scholes framework, its structural simplicity limits its ability to fit complex market-implied volatility smiles. The SABR model, with its additional parameters and ability to account for stochastic volatility and asymmetric skew, offers a more robust and flexible solution, making it better suited for modern financial markets characterized by volatility clustering and pronounced risk asymmetries.

Part III (Static Replication)

Suppose on `1-Dec-2020`, we wish to evaluate an exotic European derivative expiring on `15-Jan-2021` with payoff function given by $h(S_T) = S_T^{1/3} + 1.5 \times \log(S_T) + 10.0$ as plotted below:

We have $h'(S_T) = \frac{1}{3}S_T^{-\frac{2}{3}} + \frac{3}{2}S_T^{-1}$ and $h''(S_T) = -\frac{2}{9}S_T^{-\frac{5}{3}} - \frac{3}{2}S_T^{-2}$. To compute suitable values of $\sigma = \sigma_{\text{MF}}$ corresponding to SPX and SPY under each of the Black-Scholes, Bachelier and SABR models, we substitute the relevant results from Parts 1-2 to the formula for the derivative contract:

$$V_0 = e^{-rT}h(F) + \underbrace{\int_0^F h''(K)P(K)\,dK}_{\text{put integral}} + \underbrace{\int_F^\infty h''(K)C(K)\,dK}_{\text{call integral}},$$

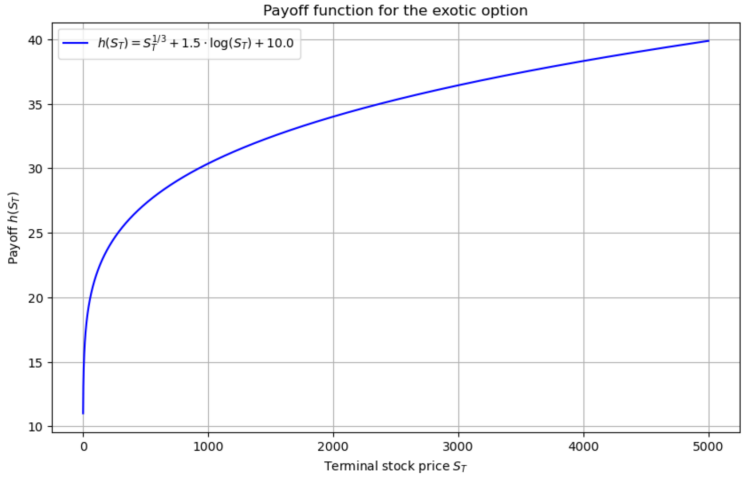

as well as the "model-free" integrated variance equation under static replication:

$$E = \mathbb{E}\left[\int_0^T \sigma_t^2 \, dt\right] = 2e^{rT}\left(\int_0^F \frac{P(K)}{K^2}\, dK + \int_F^\infty \frac{C(K)}{K^2}\, dK\right).$$

Using the Gaussian quadrature rule (coded as `quad`) for numerical integration, we obtain the following results:

	SPX (BS)	SPY (BS)	SPX (Bachelier)	SPY (Bachelier)	SPX (SABR)	SPY (SABR)
V_0	37.670	25.963	37.703	25.978	37.506	25.993
E	0.0184	0.0248	0.0052	0.0151	0.1873	0.0060
σ^2_{MF}	0.149	0.201	0.042	0.123	1.519	0.049
σ	0.386	0.448	0.205	0.350	1.233	0.221

To further investigate the robustness of the SABR model, sensitivity analyses of V_0 and σ were conducted on the calibrated parameters (see below for the plots). Variations in α, which represents the initial volatility

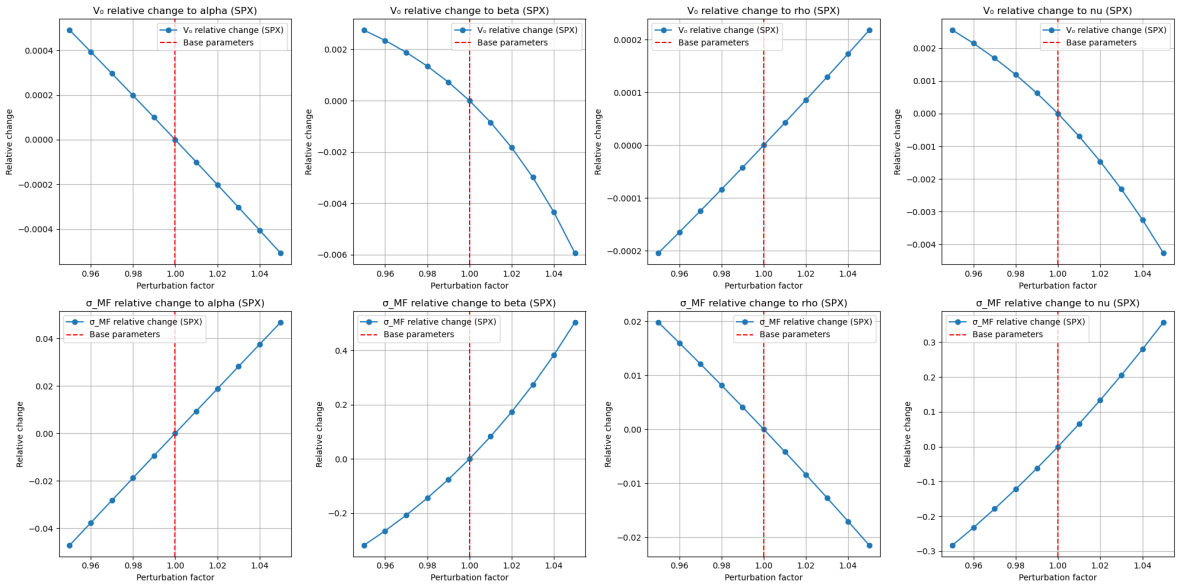

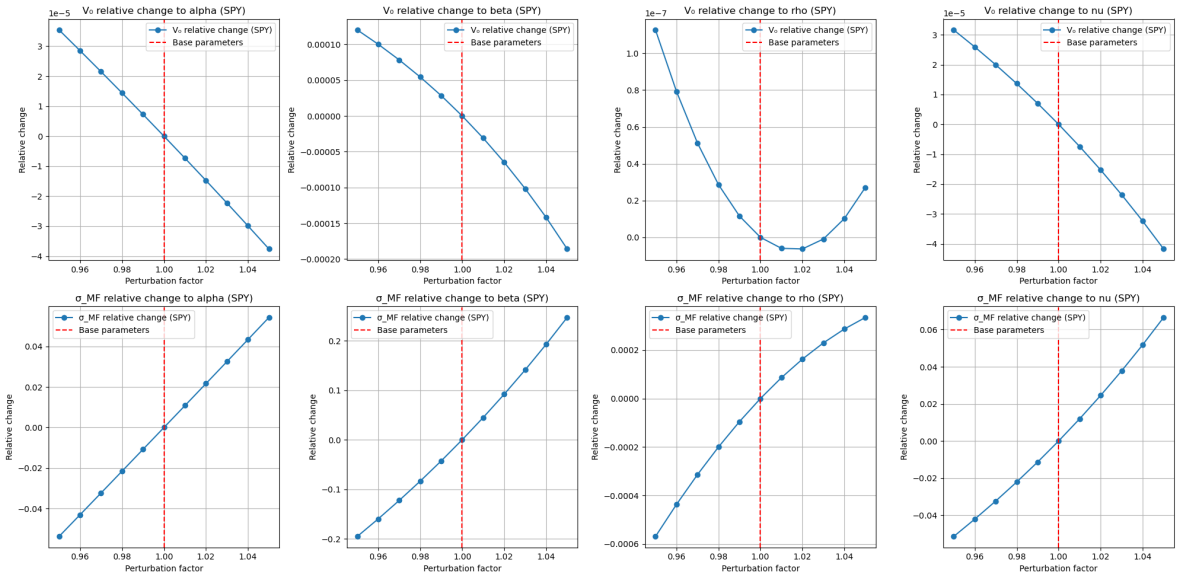

level, show that increasing α leads to a moderate increase in both the derivative price V_0 and the model-free variance $\sigma^2_{\text{MF}}T$. Sensitivity to β, which determines the elasticity of volatility, reveals that higher β slightly decreases the derivative price due to reduced convexity in the volatility surface, with effects becoming more pronounced at extreme perturbations near the factors 0.95 and 1.05. Changes in ρ, the correlation between the asset price and volatility, show a roughly linear relationship with V_0, where increasing ρ reduces the derivative price and the model-free variance, reflecting lower volatility clustering. Finally, ν, the volatility of volatility, significantly impacts the model-free variance, especially for large perturbations, but has minimal effect on the derivative price V_0, suggesting that the payoff structure is less sensitive to extreme changes in volatility dynamics. Overall, the pricing results align closely, underscoring the three models' reliability for evaluating exotic derivatives. The SABR model, with its stochastic volatility framework, demonstrates particular strength in capturing tail behavior and volatility clustering, making it well-suited for static replication of the given payoff function. The sensitivity analysis highlights the nuanced effects of SABR parameters, emphasizing the importance of precise calibration for accurate derivative pricing.

Part IV (Dynamic Hedging)

Black-Scholes introduced the notion of dynamic delta hedging − by executing delta hedges instantaneously, we ensure that our portfolio is delta neutral, and consequently hedged the exposure of our call position using the underlying stock and the risk-free bond. Suppose $S_0 = 100$, $\sigma = 0.2$, $r = 5\%$, $T = \frac{1}{12}$ year, i.e. 1 month, and $K = 100$. Suppose we sell a stock's ATM call option under the Black-Scholes model, and we hedge it N times during its life. The dynamic hedging strategy for an option is $C_t = \phi_t S_t - \psi_t B_t$, where $\phi_t = \frac{\partial C}{\partial S} = \Phi\left(\frac{\log\left(\frac{S_t}{K}\right)+\left(r+\frac{1}{2}\sigma^2\right)(T-t)}{\sigma\sqrt{T-t}}\right)$, and $\psi_t B_t = -Ke^{-r(T-t)}\Phi\left(\frac{\log\left(\frac{S_t}{K}\right)+\left(r-\frac{1}{2}\sigma^2\right)(T-t)}{\sigma\sqrt{T-t}}\right)$. Assuming there are 21 trading days over the month, we consider two different numbers of steps: 21, 84 (four trades per trading day); to simulate the stock price. By performing Monte-Carlo simulations involving 5×10^4 paths using `simulate_Brownian_Motion(paths, steps, T)` on our Jupyter Notebook, we obtain the required hedging error plots and PnL histogram (see the next page).

The analysis of the dynamic delta hedging strategy reveals several important findings regarding the behavior

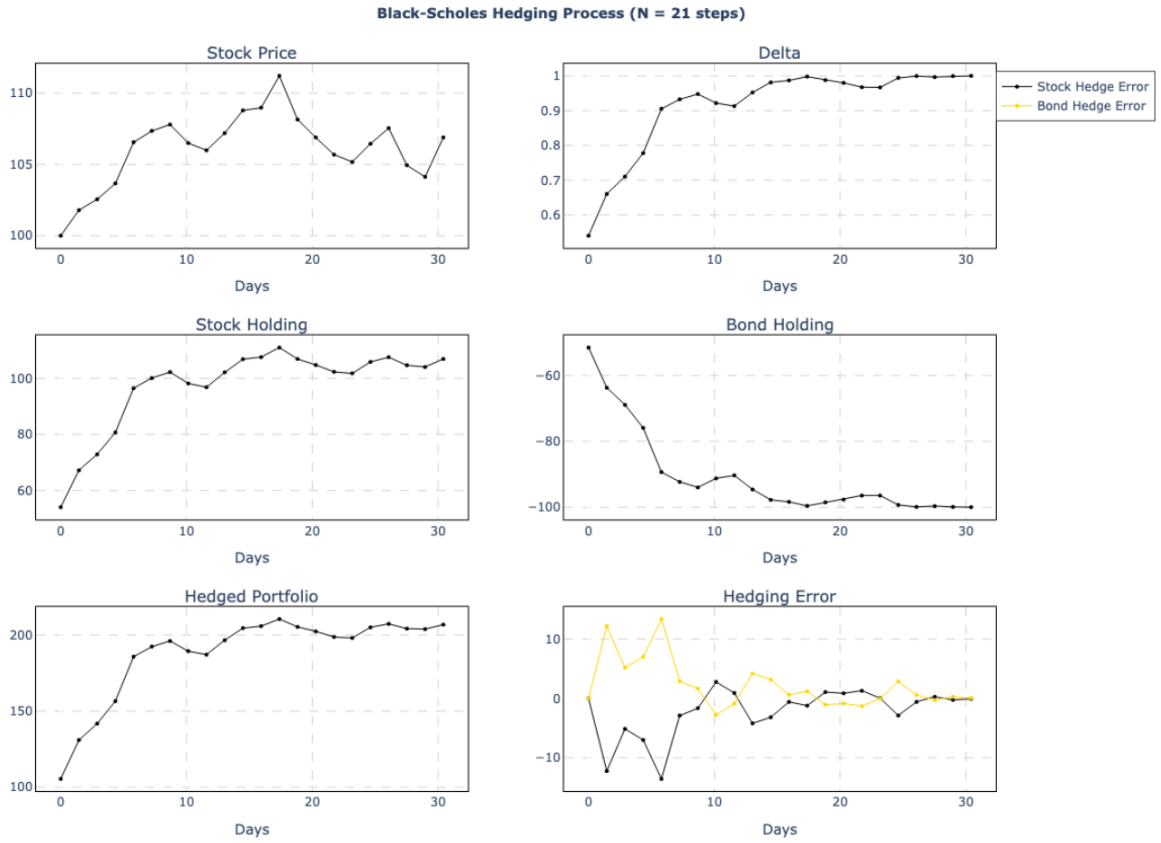
Black-Scholes Hedging Process (N = 21 steps)
Stock Price
Delta
Stock Holding
Bond Holding
Hedged Portfolio
Hedging Error
Stock Hedge Error
Bond Hedge Error
Days

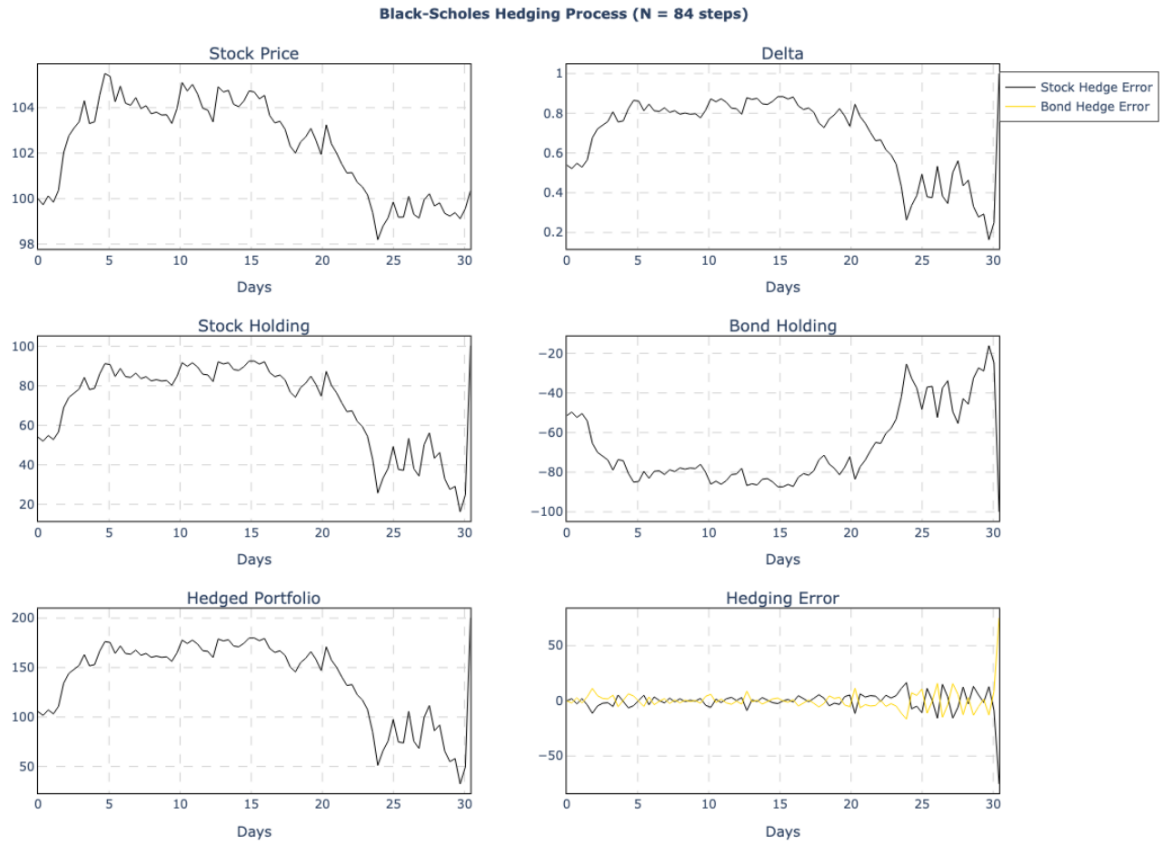
Black-Scholes Hedging Process (N = 84 steps)
Stock Price
Delta
Stock Holding
Bond Holding
Hedged Portfolio
Hedging Error
Stock Hedge Error
Bond Hedge Error
Days

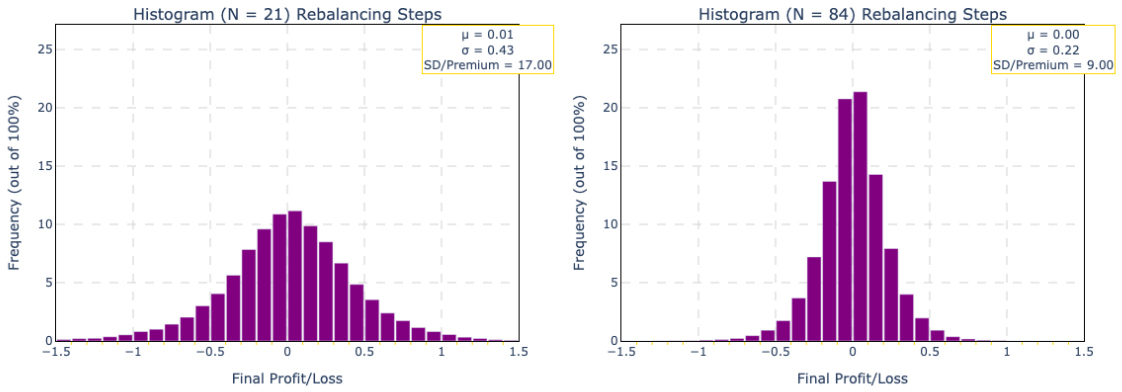

of hedging processes and the associated profit and loss distributions. The Black-Scholes hedging process was simulated for $N = 21$ and $N = 84$ rebalancing steps, representing daily and sub-daily hedging frequencies, respectively. The stock price paths, generated using a geometric Brownian motion model, exhibit random fluctuations consistent with the assumed volatility ($\sigma = 0.2$). Both simulations show similar trajectories for stock prices, affirming the consistency of the simulation model. Delta (ϕ_t), representing the sensitivity of the call option price to changes in the stock price, starts near 0.5 for the at-the-money option and decreases as maturity approaches. With $N = 84$, the delta trajectory is smoother, reflecting the finer adjustments made due to more frequent rebalancing. Stock and bond holdings also demonstrate dynamic behavior throughout the option's life. Stock holdings, defined as $\phi_t S_t$, decrease as delta diminishes towards maturity. Correspondingly, bond holdings ($\psi_t B_t$) adjust to maintain the hedged portfolio. For $N = 84$, the more frequent adjustments result in smoother transitions in stock and bond positions, whereas the trajectories for $N = 21$ are more step-like. The hedged portfolio value fluctuates around zero for both cases, indicating the strategy's effectiveness in offsetting exposure to stock price movements. However, the hedging errors − measured as the deviations in stock and bond holdings − exhibit higher variability for $N = 21$ compared to $N = 84$, further demonstrating the advantage of higher rebalancing frequency in minimizing errors. The PnL distributions, represented by histograms of hedging errors, provide additional insights. For both $N = 21$ and $N = 84$, the mean profit and loss are approximately zero, indicating that the hedging strategy successfully neutralizes exposure over multiple simulation paths. However, the standard deviation of the profit and loss is significantly different, with $\sigma = 0.43$ for $N = 21$ and $\sigma = 0.22$ for $N = 84$. This reduction in variability underscores the improved accuracy of the hedging strategy with increased rebalancing frequency. Additionally, the ratio of the standard deviation to the option premium (SD/Premium) decreases from 17.00% for $N = 21$ to 9.00% for $N = 84$, further confirming that higher rebalancing frequency effectively reduces hedging errors.

These findings highlight the critical role of rebalancing frequency in dynamic delta hedging. Increased rebalancing frequency, as seen with $N = 84$, leads to substantial reductions in hedging errors, as evidenced by smoother error trajectories and narrower profit and loss distributions. However, this improvement comes with the practical consideration of higher transaction costs, which must be weighed against the benefits of enhanced hedging accuracy. The results also validate the assumptions of the Black-Scholes model in the context of delta hedging, particularly the effectiveness of continuous rebalancing in achieving theoretical hedging efficiency. Overall, this analysis demonstrates the efficacy of dynamic delta hedging and emphasizes the trade-offs between rebalancing frequency, accuracy, and transaction costs in practical implementations.